PLASMA-DISCHARGE CONTROL IN FLUIDICS

V. Tesař, J. Šonský

Institute of Thermomechanics of the Academy of Sciences of the Czech Republic v.v.i., 182 00 Praha, Dolejškova 5, Czech Republic

Abstract

A transducer controlling fluid flow by electric signals without the two-stage conversion involving moved or deformed components have been so far unrealisable. Authors solved the problem by means of "ionic wind" of non-temperature plasma discharge acting inside a fluidic diverter amplifier. Experiments demonstrated good performance at high frequencies $f > 100$ Hz and small Reynolds numbers $Re < 1000$.

Keywords: fluidics, plasma discharge, dielectric barrier

1. Introduction

Both electronic and fluidic devices owe their advantages to the absence of mechanical moving components they both possessed in their prehistory, when electric signals were controlled by mechanical relays and fluid flows were handled by hydraulic or pneumatic valves. Analogous to the advantages obtained in early history of electronics by development from relays to no-moving-part vacuum tubes and transistors, also fluidics acquired its development momentum when it was found possible to control powerful fluid flows without any intermediate mechanism by a quite weak input. Initially, the main advantage was capability of faster response - without inertia of the mechanical components. Other advantages are less expensive manufacturing of the devices, their ruggedness, immunity to external accelerations, higher reliability, and longer life.

Many fluidic systems require being controlled - usually by an electronic controller. This is particularly true in microfluidics, where recent development in micro-machining manufacturing methods has led to broad-scale collaboration of electronic and fluidic circuits, made together on the same substrate chip. The control necessitates availability of an electro/fluidic conversion, which ideally should be also performed by a transducer operating without moving or deformed mechanical components. Unfortunately — apart from a few extraordinary cases of very special liquids, such as suspensions with electro-rheologic or ferromagnetic properties — no-moving-part transducers do not exist because ordinary most often used fluids like air or water do not respond to electric current or voltage inputs. As a result, standard transducers nowadays operate in two-stage manner, converting first the electric input into mechanical movements – which then, in turn, influences the fluid flow. This intermediate step means the advantages of electronics and fluidics are lost in the devices mediating their collaboration.

2. Principles of E / F non-thermal plasma action

2.1 Intermediate mechanical transducers

At the earliest stages of its history, fluidics was so much fascinated by then newly discovered capability of flow control without mechanical components — and the consequent freedom from the limits imposed by inertia — that it was seriously considered a competition to electronic information processing. After all the competing electronics has at that time just passed through the analogous development step of discarding the relays as active devices (the first computers processed the signals by mechanical relays). Electronics won the competition because of its offer of smaller size (fluidics requires operation above a certain Reynolds number which limits the minimum size scale) and higher speed of electronic devices (fluidics is limited by speed of sound – while in electronics it is the speed of light). This relegated fluidics to those applications where the fluids have to be handled anyway – like, e.g., in the search for new drugs or catalysts [1] where the samples very often come in liquid or gas form. The overall control of the systems is almost always the domain of electronics calling for electro/fluidic signal transducers, preferably possessing the same characteristic properties (in particular the output loading characteristic) as fluidic devices to simplify the mutual matching of devices as the key step in circuits design.

Unfortunately, as already mentioned above, the E/F conversion is exactly one of those transducing problems where a direct conversion has been so far resisting all attempts at a satisfactory

solution. Currently used standard transducers are based on indirect two-stage E/M/F conversion [2], with mechanical motion as the intermediary step. Typical devices used in the transducer role are solenoid valves, with the acting mechanical organ moved electromagnetically. Of whatever design, electromagnetic transducers are inherently voluminous, heavy, difficult to accommodate on the circuits substrate, and possessing disadvantages of limited life and reliability (e.g. their springs may be broken due to material fatigue). They cannot withstand temperatures as high as fluidic devices do when made from refractory materials.

Nearer to the desirable solution is another family of transducers, based on the "guided jet" principle [3, 4]. The mechanical organ, which is not moved but deformed, is minimised to a very narrow thin strip fixed at its one end inside the supply nozzle. The device has the geometry of typical fluidic jet-deflection diverter amplifier, supplied with the fluid which in the supply nozzle forms a jet – to which the strip attaches by the Coanda attachment effect. Deformation of the strip by electrically generated force varies the direction of the jet which continues in the deflected direction after having left the strip end, where it enters one of the collectors that captures the jet as they do in ordinary fluidic amplifiers. The advantage is minimal size (and, hence, minimal inertia) of the moving component. Additional advantage is compatibility of the fluidic impedance properties with fluidic jet-type active elements. Problematic remains generation of the force that acts on the strip. It may be produced by an electromagnet but this means inheriting many of the above-mentioned disadvantages brought by solenoid valves. A better solution is to set-up the guided jet device with a bending piezoelement [5, 6] which takes the role of the deflected strip. The problem is quite small bending angle and high required input signal voltage.

Probably the only case of complete absence of moving mechanical organs are transducers with electrically heated attachment wall. Again, the basic body of such transducers corresponds to that of a bistable diverter fluidic amplifier (usually without control nozzles). The principle of operation is based upon the fact that an air jet ceases to be attached to attachment wall when the latter is heated [7] . Unfortunately, the responses are generally too slow because of thermal capacity lag.

2.2. Control action by non-temperature plasma

The idea discussed in the present paper is no-moving-part control of air flow in a fluidic jet-type device by plasma discharge deflection of the jet. The discharge occurs in the air between a pair of electrodes if dielectric strength of air is surpassed so that some molecules are decomposed into ions and free electrons. These particles carry electric charges and this makes them responsive to electric field. The discharge phenomenon was first described by Sir W. Crookes in 1879 and the character of the ions and electrons was identified by J. Thomson in 1897. The name “plasma” was given to the ionised state by I. Langmuir in 1928. Depending on the relative energy – expressed by equivalent temperature – of the ions, electrons, and remaining neutral molecules, the plasma is described as thermal or non-thermal. It is called thermal if these components are in thermodynamic equilibrium — which occurs at extremely high temperatures. The plasma generated in the transducers discussed in this paper is called non-thermal because the ions as well as the neutral molecules are at room temperature while the motion of electrons, not in equilibrium with them, corresponds to a very high temperature. What is used to deflect the air jet in the discussed electro/fluidic signal conversion devices is the so called “ionic wind”. It is created by acceleration of air molecules by collisions with the fast-moving electrically charged particles.

Using this air "wind" to influence aerodynamic phenomena such as, e.g., generation of lift, is not a new idea – it was patented already 1950s and 1960s [8, 9, 10]. Especially Roth’s patent [11] and book [12] became the basis upon which many later researchers built their investigations. The effect they aimed at was control of flow past bodies or airplane wings [13], mainly by influencing boundary layer. Initially, attention concentrated on the corona wind. It was generated with the configuration of electrodes as shown in Fig. 1, characterised by one electrode in the form of a sharp point. The electric strength of air above which ionisation takes place is defined by a certain limiting value of electric field gradient. This gradient reaches very high values near the sharp point due to the radial convergence of filed lines. In a popular version the large-surface electrode had the form of a ring, with the sharp electrode on its one side, the axial jet formed at the other side. The ring thus had the role of "nozzle". The flow from it was planned to influence flow separation or laminar/turbulent transition as in the case of standard air jets. The success was limited due to too low velocities, insufficient for momentum action of the controlled air flow. Development has led to closing the ring on the inlet side and apply the electric input to form inside the ring sparks at low repetition frequency. Each spark discharge generates on the outlet side a heat pulse, heating the cavity contents and pushing it out – alternating with the suction pulses during which the outer air enters the cavity — in a manner well known as the principle of synthetic jet [28]. In several aspects

this approach utilizes the large amount of experience obtained with development of spark plugs for ignition type internal combustion engines [29].

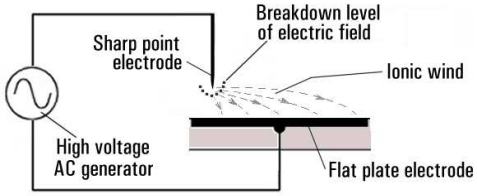

Figure 1: Corona discharge – the earliest version of non-thermal, atmospheric pressure plasma discharge. One electrode is a sharp point near the tip of which the electric field intensity surpasses (because of radial convergence) the dielectric strength of air, which thus becomes ionised. The charged particles, driven by the electrostatic force, collide with neutral molecules of air, generating the ionic wind.

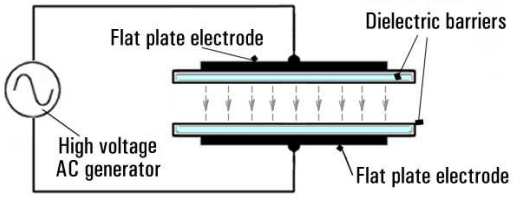

Figure 2: Dielectric barrier discharge in its classical symmetric configuration. Both electrodes are covered with a layer of dielectric material.

Interest in the non-thermal discharges remained, mainly due to its promise of needing a lower electric input. It was, however, turned towards the different discharge configuration, the dielectric barrier discharge. This is also the result of high AC voltage applied between two electrodes, surpassing the dielectric strength of air. The earliest layouts had originally [12] both electrodes covered by the dielectric barrier coating, as shown in Fig.2. The barriers limit the electric current and prevent formation of sparks. The pursued aim remained an application to control of boundary layers on bodies and wings surfaces. For this purpose, however, the basic symmetric configuration of Fig. 2, with the ionic wind perpendicular to the dielectric barrier surface, is not directly applicable. Also the presence of the top electrode is not acceptable if the controlled boundary layer should be under it.

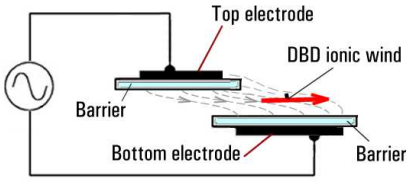

Figure 3: Asymmetric dielectric barrier discharge generates the ionic wind parallel to the electrode surfaces. In principle is this configuration useful for producing a flow in a channel with parallel walls.

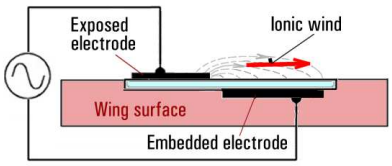

Figure 4: Electrode configuration nowadays used as more or less standard for DBD control of boundary layers. Electrodes share a single dielectric barrier and the exposed electrode may be of practically negligible thickness, vacuum deposited asymmetrically on the barrier upper surface, so as not to influence the controlled boundary layer.

Ionic wind flow more suitable - possessing a velocity component parallel to the surface - may be obtained with the asymmetric configuration presented in Fig. 3, although the problem with the counter-electrode presence above the surface still remains. The solution was in minimising this electrode thickness and placing it directly above the dielectric barrier which may be only single one. The resultant configuration is in Fig. 4. The idea caught on, due to obvious simplicity of the actuators for influencing boundary layer - and also the relatively less demanding electric input circuit. Roth [11, 12] coined for it the acronym OAUGD ("*one atmosphere uniform glow discharge surface plasma*"). It soon led to many publications presenting experimental verification of various versions. Many results are summarised in the surveys like [14] and [15]. The acronym currently much more often used (outside the Roth's team) is DBD – "*dielectric barrier discharge*". Practically all extensive research effort currently concentrates on control in external aerodynamics, i.e. action on boundary layer — apart from a few studies of flow separation in diffusers, which is closely related. The only known case of applying DBD to flow control fluidics is ref.[16]. The idea pursued there was influencing the constant cross-section channel flow by the corona wind at one of the walls of channels leading to the control nozzles of a fluidic amplifier. Because

of the quite small velocities that may be generated by DBD, the effects described in [16] are not very impressive.

2.3. The layout chosen for use in fluidics

The configuration of electrodes and ionic wind trajectories selected by authors for their experiments is presented schematically in Fig. 5. It possesses a mixture of features. From the corona discharge principle in Fig. 1 is inherited the very small electrode exposed to the controlled air flow. It is here combined with the dielectric barrier discharge principle from Figs. 2, 3. The exposed electrode is inside the interaction cavity of the fluidic device, while the other, large-surface area electrode covered with the dielectric barrier is encapsulated inside the material of the device body. The transducer bodies have to be, of course, of non-conducting material and some manufacturing advantages may be obtained if this material has high dielectric constant and strength, so that its layer at the bottom of the cavity may directly serve as the dielectric barrier. The other, exposed electrode could be a thin and narrow vacuum-deposited metallic layer – or, as was the case in the tests, it may be a thin wire passing through the air-flow cavity. It initial tests it could be placed to different heights h above the floor of the cavities in the transducer device. The generated ionic wind flows from this exposed electrode towards the asymmetric, horizontally shifted encapsulated electrode in a direction that has a significant velocity component parallel to the cavity floor.

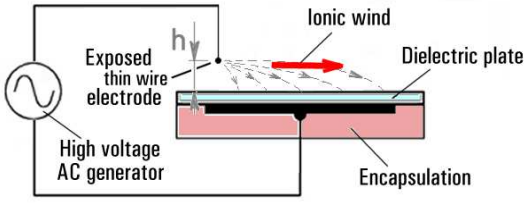

Figure 5: Employed by the present authors was the hybrid configuration, in-between corona discharge (Fig. 1) and dielectric barrier discharge (Figs. 2, 3). The wire electrode height h was in the latest experiments decreased to h = 0 (i.e. placed on top of the dielectric barrier).

In the first tests, the electrode was at height h > 0. It was a thin metal wire passing through a drilled hole in the device body at about half-way to cavity depth so that its exposed part traversed the interaction cavity. Later a simpler to manufacture layout was with the wire placed on the cavity floor.. In the first case it was expected the signal conversion will be more efficient, the generated ionic wind interacted with the controlled air flow in a larger volume and thus acted on more neutral air molecules. The disadvantage, on the other hand, was that this inevitably resulted in a larger mutual distance between the electrodes. The lower magnitude of the electric field gradient resulted in lower ionic wind velocity. The second case was easier to make, the very thin wire in its non-exposed part was simply pressed to the surface of PMMA material. Of course, the generated ionic wind then occupied only a small layer of the cavity. Nevertheless, experience has shown that the performance of the test model was in this case evidently higher. It was therefore this wire position that was used and the data in this paper were all obtained with this h = 0 case.

2.4. The basic contradiction

Working with high voltage is obviously a complication and there are very good reasons to design the transducer for working with voltages as low as possible. On the other hand, the general disadvantage of ionic wind in performed tests and in literature is its velocities are lower than desirable. There is, unfortunately, no escaping from the basic contradiction: the velocities increase with increasing gradient of electric field and this means increasing applied voltage difference between the electrodes. The basic relations between these two contradictory requirements may be demonstrated by simplified analysis.

The relation between the basic requests of minimum voltage difference ΔU [V] and maximum ionic velocity w_{iw} [m/s] may be evaluated by simplified one-dimensional description. The derivation begins by the expression for the simplest capacitor with flat plate electrodes and a dielectric barrier between them. The electrodes are pulled together by the electrostatic force per unit of surface area – i.e. the electrostatic pressure ΔP [Pa]

$$\Delta P = \frac{\varepsilon_0 \varepsilon \, \Delta U^2}{2 s^2} \qquad (1)$$

where $\varepsilon_0 = 8.85\ 10^{-12}$ F/m is permittivity of empty space, ε [-] is dielectric constant of barrier material, s [m] is barrier thickness, and ΔU [V] is the amplitude of applied AC voltage. Admittedly, eq.(1) is strictly valid for a different configuration than that of Fig. 5. The one-dimensional approach assumes the configuration similar to Fig. 2 (simplified by zero thickness of air gap and the barrier reduced to a single

plate). Nevertheless, as a rough estimate may be eq. (1) quite useful. The next simplification is equating the pressure ΔP with the dynamic pressure of air flow

$$\Delta P = \frac{w_{iw}^2}{2v} = \frac{\varepsilon_0 \varepsilon \Delta U^2}{2s^2} \tag{2}$$

- where v [m^3/kg] is specific volume of air. Thus the ionic wind velocity should be

$$w_{iw} = \Delta U \sqrt{\varepsilon_0 \varepsilon v}/s \tag{3}$$

Of course, this prediction is too optimistic. The ionic wind cannot traverse the shortest distance between the electrodes (as in Fig. 2) and has to follow more complex paths. This makes the local voltage gradients values smaller – and also smaller local velocities. Considering all simplifications, the expression eq. (3) for the velocity w_{iw} has to be corrected by a very small correction factor c_w

$$w_{iw} = c_w \Delta U \sqrt{\varepsilon_0 \varepsilon v}/s \tag{4}$$

Experience has shown that magnitudes of the correction factor are of the order $c_w \sim 0.1$I

At any rate, eq. (4) demonstrates that minimising w_{iw} cannot be made together with maximising ΔU. What may seem to be a way out from this contradiction in eq. (4), choosing very small barrier thickness s, is also no perfect solution since the very thin dielectric cannot withstand higher gradient than the limiting dielectric strength $\Delta U_{max} / s_{min}$ of electric breakdown. In air its value is

$$\Delta U_{max} / s_{min} = 3.0 \text{ V/m} \tag{5}$$

Some dielectric materials have much higher strength, e.g. PMMA

$$\Delta U_{max} / s_{min} = 25 \text{ V/m} \tag{6}$$

- but this is not really helpful because the ionic wind trajectories must traverse the controlled air flow. Choosing a different gas is hardly a choice – some gases cannot be simply ionised an may be inacceptable in the fluidic part of the system. Dielectric constant of air is practically $\varepsilon = 1.0$ and together with the specific volume v cannot be reasonably manipulated. At any rate, the two gas parameters v and ε are in eq. (4) under the square root symbol, indicating poor improvement even if a suitable gas is found.

3. Transducer principle

3.1. Starting point of development

Present authors' development of the E/F transducer was based on the idea of adapting— by addition of the electrodes — a popular fluidic active device, the bistable fluidic diverter valve. A typical representative is shown in Fig. 6. This device is an amplifier since it delivers a quite powerful flow from its output terminals in response to a weak control flow, injected through the control nozzles. The supply flow from an external source is in this amplifier not turned down by the control action but instead it is diverted between one of the two output terminals. The switching of the main jet by the flow from the control nozzle is in the transducer to be replaced by action of the ionic wind, achieving the same effect.

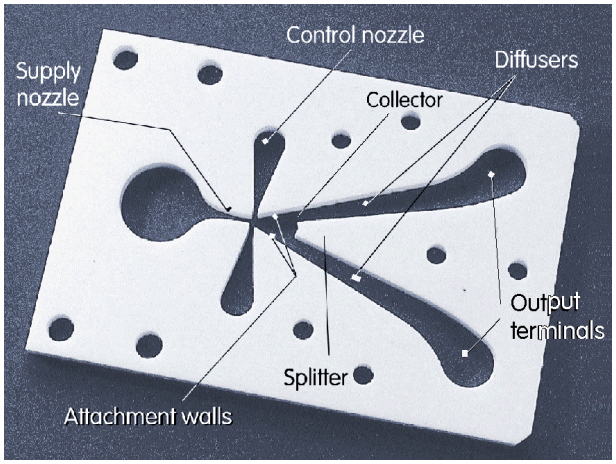

Figure 6: An example of the main plate of a fluidic bistable diverter amplifier. It was used as the starting point in the development of E/F transducer. Air flow cavities were laser-cut in teflon. Air supplied through the supply nozzle at left forms a jet which attaches by Coanda effect to one of the two attachment walls and is captured by collector. After pressure recovery in the diffuser the air flow leaves through one of the two output terminals at right.

The diverter amplifier shown in Fig.6 is bistable. This means it tends to assume one of the two stable regimes - and return back into this regime after cessation of a disturbance (apart, of course, a

disturbance sufficiently strong applied in a control nozzle on the active side of the device, which would switch the device into the other, equally stable regime). The advantage of the bistability is decreased requirements of necessary control power. The amplifier does not need a continuous input control flow but the switching between the two regimes is done just by short control flow pulses. After each pulse the control flow may stop and yet the air jet remains deflected. The bistability may be directly useful for collaboration with binary electric signals. If it is to be used for task requiring a continuous variation of the output air flow rate, the solution is to operate the device in the PWM (pulse width modulation) control regime – with variable length of the time during which the air enters the same output terminal.

The character of the flowfield inside the amplifier is presented schematically in the next Fig. 7. Shown there is the state with absent control flow (and also absent control nozzles, drawn therefore in Fig. 7 by dotted lines). Despite the symmetric geometry of the cavities, the flowfield inside the amplifier is asymmetric. The jet is deflected by the Coanda attachment effect to one of the two walls positioned at the opposing sides of the interaction cavity. The wall to which the jet is attached at a particular time is described as the active one. The fluid leaves the device through the output terminal on the active side. The attachment is essentially a result of jet-pumping effect which is caused by entrainment of the surrounding fluid into the jet. This pumping meets different conditions on the two sides of the jet. On the inactive side, the entrained fluid is replaced without problem by fluid entering through the inactive output terminal. No such replacement is possible on the active side, where between the jet and the attachment wall is formed a closed recirculation bubble. Formation of the bubble is assisted by the small adaptation of geometry resulting in the setback (Fig. 7). The fluid removal by entrainment from the recirculation bubble causes there low pressure. The deflection of the jet is due to the pressure difference between this low pressure on the active side and higher pressure on the inactive side.

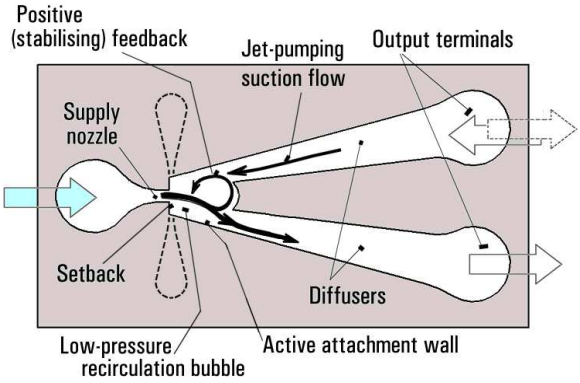

Figure 7: Basic character of the flowfield inside the amplifier shown in Fig. 8 in a regime with no control flow (control nozzles, not needed in the transducer, may be removed – at least in principle). Bottom half of the amplifier, with the main jet diverted there, is described as active.

Of importance for the following discussion is the fact that the intensity of the jet-pumping entrainment depends on the magnitude of jet Reynolds number. If at a high Re the jet is fully turbulent, the efficiency of entrainment is high. Outer air is dragged along with the jet by entering the spaces between the vortical structures that are generated on the jet outer edge. There are no such vortices at low Re regime and, consequently, the Coanda effect then ceases to be efficient because the entrainment into a laminar jet is very small. Once the laminar jet is curved, however, the laminar/turbulent transition becomes promoted by pathline curvature – cf., e.g., [18]. The Coanda-effect devices are thus capable of operating at Reynolds numbers significantly lower than those typical for the transition in straight submerged jets.

The splitter between the two collectors is presented in Figs. 6 and 7 being of bicuspid shape. Between its two sharp cusps is a concave wall. As shown schematically in Fig. 7, this wall shape generates a stabilising feedback action that assists the Coanda effect (and, at least to some degree, can actually replace it). If the main jet flow would try to separate from its active attachment wall, the cusp nearer to this wall peels off outer layer from the jet (this is shown in Fig. 7) and directs it back towards the nozzle exit, i.e. into the location where the jet can be effectively acted upon. The "peeled-off" feedback flow tends to bend the main jet towards the active attachment wall and stay at it. This is also an effect that may be present even at quite low Reynolds numbers where the attachment to the wall would otherwise be weak.

3.2 Electrodes

With their two input and two output terminals, the fluidic amplifier in Figs. 6 and 7 may seem to be, in a certain sense, a combination of two amplifiers with common supply inlet terminal. One of these amplifiers is in the active state, the other is inactive. Thus the ionic wind generating transducer based on

this amplifier principle also has to contain essentially two electrode systems - each of them corresponding to Fig. 5. In the tested configuration both systems have one common (grounded) electrode. Its surface must be small. In our case it is the thin wire or similar component exposed into the air flow. The two other electrodes, the encapsulated ones, are separated from the working cavities of the device by a thin layer of the dielectric barrier. The configuration shown in Fig. 5 was chosen among the alternatives described in [17] as preferable because it is simple and relatively easy to adapt from an existing amplifier design. The aim is to generate by the electric input signal the ionic wind acting transversally (i.e. perpendicularly to the main jet flow direction) upon the deflected jet, forcing it to switch from the active attachment wall to the opposite wall, that so far has been inactive.

There is a number of possible layouts of the three electrodes that can achieve the switching of the Coanda-effect attached jet. Some alternatives, as already mentioned above, were described in detail in ref. [17]. In all cases it is assumed that the material of the transducer bodies is plastic, electrically non-conductive. In some cases, this material may have suitable dielectric properties so that a thin layer of it between the channel and the electrode may serve as the dielectric barrier of Fig. 5.

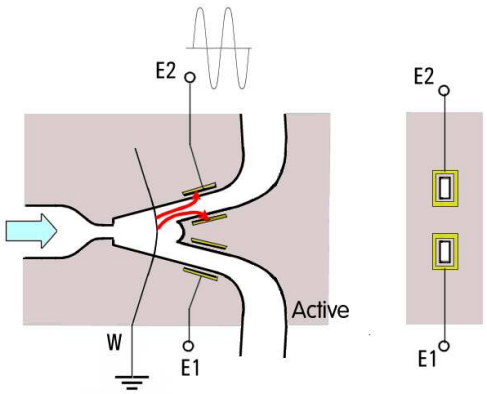

Figure 8: One of the early designs of the no-moving-parts transducer from [17]. The dielectric material of the body forms the barrier layer between the hollow electrodes (E1, E2) and exit channel walls. To switch the air flow away from the active side, the non-temperature discharge is generated by admission of high AC voltage between the wire electrode W and the inactive-side electrode E2.

One such case is presented in Fig. 8. The grounded wire electrode is located so that it passes through the interaction cavity. The two encapsulated electrodes E1 and E2 are hollow and the exit channels of the transducer pass through them. It is assumed that the device in Fig, 8 is in the state presented in Fig. 7. This means, that the air leaves the device through the bottom exit (this is why this exit in Fig. 8 it is marked as active. The AC high-voltage electric control signal is introduced to the electrode E2 and generates the ionic wind directed into the inactive exit channel. This layout has two disadvantages. First, the distance between the wire electrode W and the hollow electrode E2 is relatively large. To generate sufficient control action may need inconveniently high driving voltage. Also from the fluidic point of view this design does not look very efficient. The generated ionic wind does not act directly upon the main air jet that dominates the flowfield (Fig. 7). Instead, the ionic wind attempts to move the air jet from its active attachment wall by suction into the upper exit channel. This suction is not likely to be efficient – especially if the ionic wind is slow and hence its Reynolds number is small.

A solution of one of the problematic aspects may be the other example, presented in Fig. 9. Instead of the hollow electrodes there are flat plate electrodes reaching to a very small distance from the wire electrode W. This may result in higher ionic wind velocities. The not very effective control by suction into the inactive exit, however, remains. There are several alternative possibilities how to accommodate the flat plate electrodes into the transducer bodies The sections through the bodies at the right-hand side of the illustration Fig. 9, named a, b, and c variants show three examples. The case a shows the electrode plates immersed during the manufacturing process into the melted body material (which is assumed to have high dielectric constant to serve as the barrier). In the case b the encapsulated electrodes are only on one side, simplifying the manufacture but very likely with less efficient interaction between the controlled air jet flow and the ionic wind. The stack of plates design in the case c has the electrodes on both sides of the channels – of course, at the price of a more complex stack.

A solution of the problem of more efficient interaction between the ionic wind and the controlled air jet flow is presented in Fig. 10 — another derivation of the idea in Fig. 9. The basic difference is the placement of the exposed wire electrode W. It is in Fig. 10 placed downstream from the encapsulated electrodes. Note that in this case the high AC voltage is applied to the encapsulated electrode on the active side of the device. This forces the generated ionic wind (again shown here in red colour) into the head-on collision with the air jet.

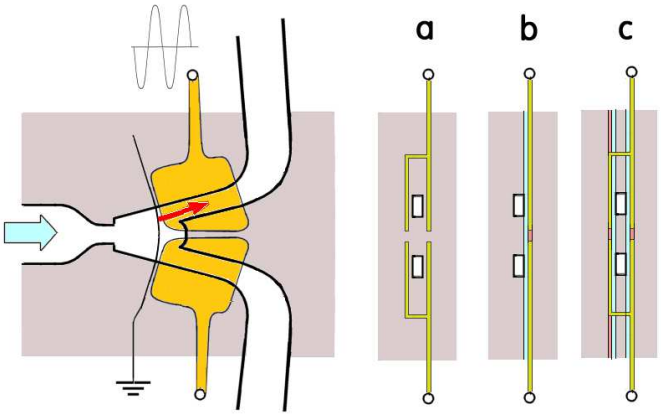

Figure 9: Alternative to the design shown in Fig. 8. The encapsulated electrodes are planar. The sections a, b, and c show possible variants of encapsulation, insertion of the dielectric-barrier plate(s), and construction from a stack of thin plates

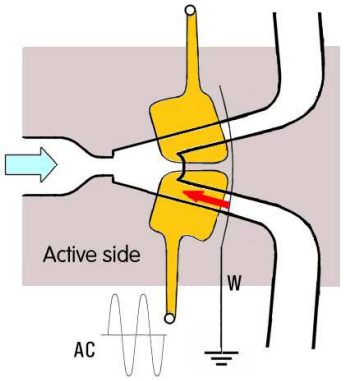

Figure 10: Another alternative of the planar electrode encapsulation – a version with the ionic wind blown opposite to the air jet. Note that the high-voltage is here applied to the active-side electrode, pushing the ionic wind into a head-on collision with the active-side jet flow. This is likely to be more effective control action method.

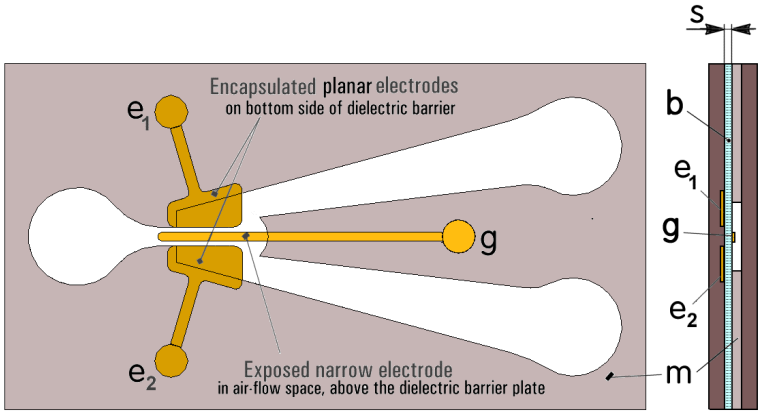

Figure 11: Another alternative from [17] of the transducer design with planar electrodes. The ionic wind acts on only inactive half of the interaction cavity. Again formed from the stack of plates containing the dielectric barrier b and the main plate m in which are laser-cut the air-flow cavities.

The shortcoming of the designs in Figs. 9, 10, and 11 is that it does not really use the amplifier properties of the basic fluidic cavities. The ionic wind acts on the main air flow downstream from the interaction cavity. To make use of the amplification capability, the ionic wind should act on the controlled air flow inside the interaction cavity.

The drawing in Fig. 11 shows the basic layout of another configuration of air-flow cavities and electrodes from [17] in which the ionic wind is indeed generated in the interaction cavity between the two attachment walls. The transducer models investigated by the present authors were a version of this idea. It should be emphasised that the reason for this choice is the fact that it was particularly easy to build from available parts spared from earlier different projects. The transducer is in this case again a stack of non-conducting rectangular plates. The cavities for the air flow were again made in one of the se plates, the main plate m. At left in Fig. 11 the plates are presented in plan view while at the right-hand side of the drawing is a cross section by a plane passing through the interaction cavity. All electrodes shown in Fig. 11 were originally designed to be made by vacuum deposition (such as, e.g., sputtering through a mask) on the barrier plate b, which serves as the floor of the air-flow cavities. As discussed below, for the feasibility tests.

For building the test models, the electrodes were actually improvised. Instead of the planned deposition by sputtering they were made as separate components inserted into the stack. The two encapsulated electrodes, e_1 and e_2 (Fig.11) were made by fixing to the bottom face of the barrier plate b two thin metal foils, simply cut into a rectangular shape. The exposed grounded electrode g was made from a short length of a very thin wire.

Since the discussed transducer, especially in its initial, extemporised form, was originally intended merely for feasibility tests, the simplicity of electrode system design was given precedence before effectiveness of ionic-wind action. As seen from comparison of Figs. 7 and 11, the generated ionic wind exists only in the inactive side of the interaction cavity. Hence, it can not influence directly the main jet, which is on the active side. It flows from the grounded electrode g in the direction perpendicular to the wire – apart from the small segment of the air jet immediately downstream from the main nozzle exit (the jet is curved and after a short travelled distance it escapes from this influence). Where the ionic wind can act quite effectively despite being on the inactive side is its effect on the positive feedback vortex, Fig. 7. It may also oppose and perhaps suppress the jet-pumping suction flow in the inactive diffuser, especially because observed trajectories of the discharges upon impingement on the inactive attachment wall tended to be bent into the inactive diffuser, where they opposed the jet-pumping inflow.

In the tested wire form, the electrode g was placed directly on top of the barrier plate b. This, of course, is another factor leading to limited efficiency. Generated ionic wind thus can influence the controlled air flow only at the surface of the barrier (i.e. the bottom of the cavities). If the wire were be lifted above the barrier top surface, the ionic wind would interact with larger part of the volume of the cavity. This, however, would place it farther away from the wire electrode and would necessitate undesirable higher voltage of the driving signal. Also, visual observation of the ionic wind in that case has shown the phenomenon of filamentation –decreased homogeneity of the discharge. Authors tried to avoid it, although it must be admitted that it is not exactly known whether or not the filamentation makes the interaction with the air flow better or worse.

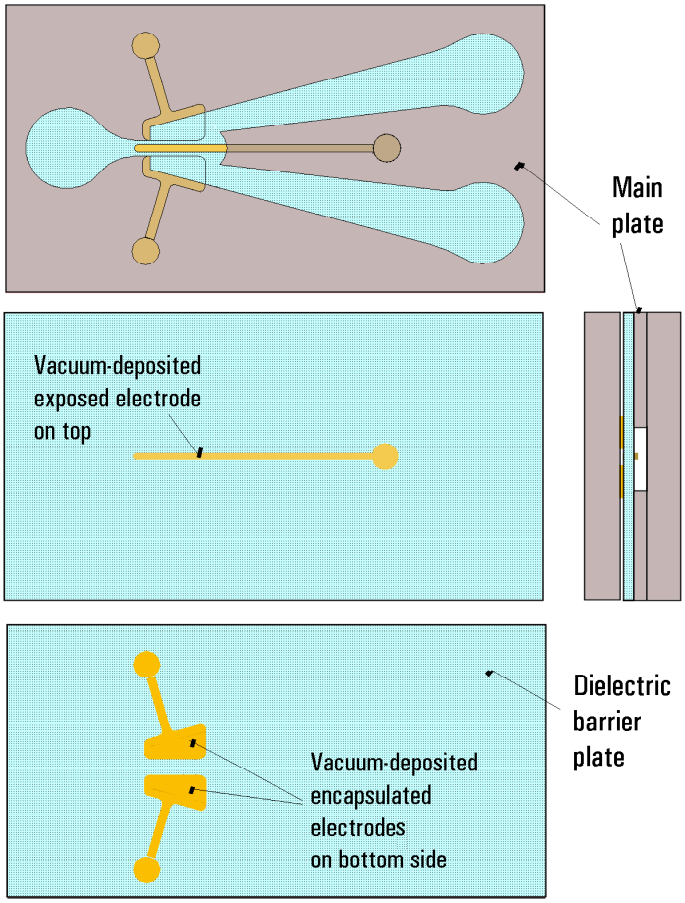

Figure 12: Important plates from the transducer in Fig. 11 assembled as a stack of rectangular plates. Electrodes were designed so as to be deposited by sputtering in vacuum (with the shape of the deposition defined by a mask) on both sides of the dielectric barrier plate.

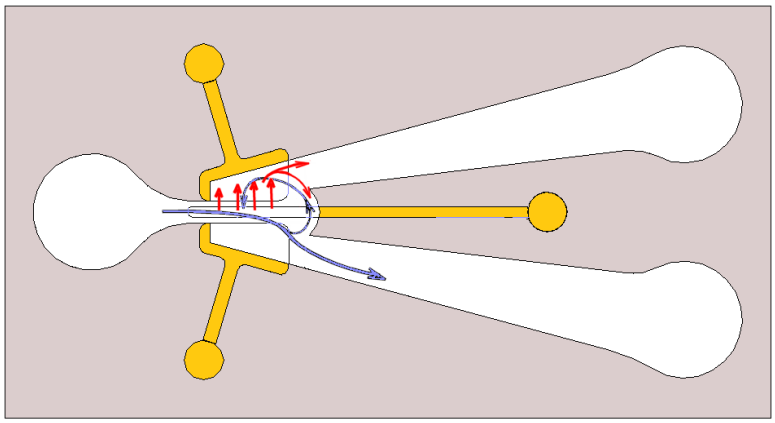

Figure 13: Comparison of the fluidic amplifier flow (blue) and the ionic wind (red) inside the device from Figs. 7 and 11. In spite of the attractiveness of this design from manufacturer's point of view, its E/F conversion efficiency cannot be particularly high because the ionic wind flow covers only one half of the interaction cavity on the inactive-side.

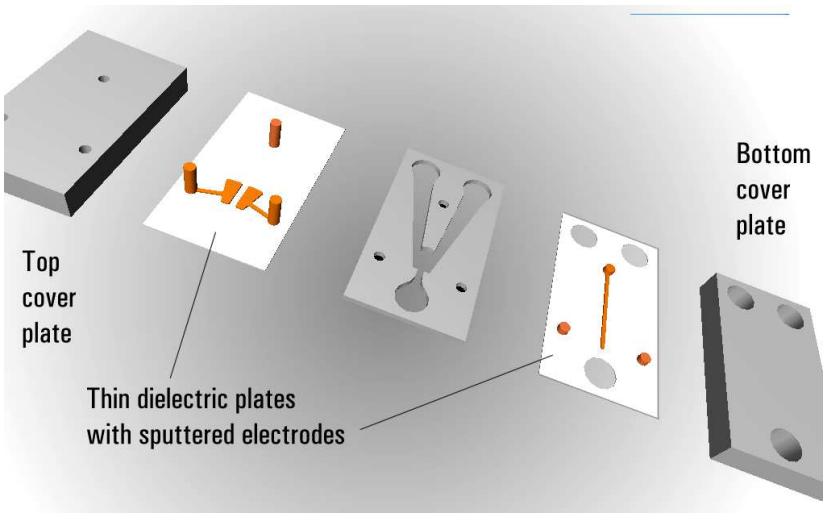

Figure 14: Expanded view of an alternative transducer version base on the same idea as in Fig. 12. Instead of placement of the electrodes on top and bottom of a single dielectric barrier plate (as in Figs. 11 and 12), here are two barrier plates. Cover plates are rather thick to secure the solidity of the assembled model.

3.3. Extemporised feasibility tests

To verify the applicability of the idea described above — especially the feasibility of operating with electrode configuration characterised by axial location of the exposed electrode and hence the ionic-wind acting predominantly in the inactive half of the interaction cavity — a simple laboratory model from available components was set up. The main component, a plate of transparent PMMA (polymethylmerthacrylate) of 2 mm thickness with laser-cut cavities of a fluidic amplifier, was available as a leftover from previous experiments with fluidic devices (in particular from tests of the quarter-wave resonator type fluidic oscillator discussed in [19]). It was placed on top of a thicker baseplate, also from the PMMA material, where it was held by screws – seen in Fig. 15.

Another essential component for building the extemporised model was the dielectric barrier. Its critical property was high dielectric breakdown strength, $\Delta U_{max} / s_{min}$ (cf. Fig. (6)) i. e. the capability of withstanding the high voltage difference ΔU between the electrodes separated by plate thickness s. Suitable plate for the role of the barrier was found in Al_2O_3 ceramic plate of size 38.1 mm x 25.4 mm (1.5" x 1") of thickness $s = 0.6$ mm, which was available originally designed as heat-sink insulation plate for a high-power transistor. The breakdown strength of Al_2O_3 is 14.5 kV/mm – less than that of PMMA (eq. (6)) but still high enough. Its dielectric constant is $\varepsilon = 9.3$ so that according to eq.(4) it may be ideally possible to obtain maximum ionic wind velocity as high as $w_{iw} = 12$ m/s - assuming $c_w \sim 0.1$. Other advantages of the Al_2O_3 material is relatively high thermal conductivity and small thermal dilatation, which provided a useful perspective for resistance to thermal breakage in the high local heating conditions at the electrode wire if it were placed on top of the barrier surface.

Geometry of the cavities in the main plate is presented in Fig. 17. The original purpose of the main plate with the cavities was its use in a fluidic oscillator with resonator cavity. According to [19] the resonator channel was arranged as a continuation of one of the control nozzles inlet. Not needed for the present purpose, most of this resonator part was cut off. The control nozzles, theoretically also

superfluous, were retained. In fact a test of closing the control nozzles opening into the atmosphere has led to obvious deterioration of the performance.

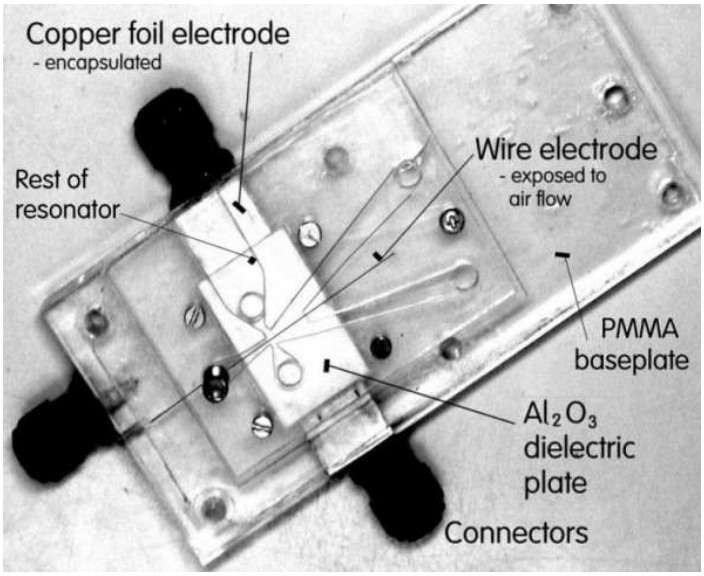

Figure 16: Photograph of the first transducer model extemporised from an existing bistable diverter. Descriptions of details of the feasibility study model. The narrow exposed electrode is here the grounded wolfram wire, passing through the interaction cavity. The two side-by-side electrodes under the dielectric barrier plate are thin copper foils. Good performance was obtained thanks to the favourable properties of the dielectric barrier plate.

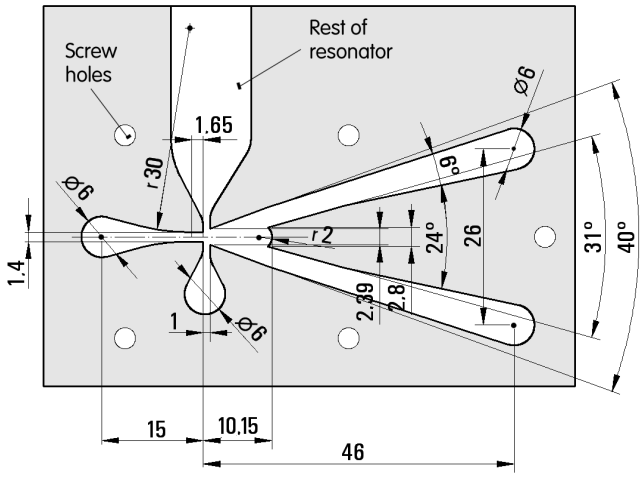

Figure 17: Geometry of the second model. Because of favourable previous experience with the extemporised first model (Fig. 17), the key parts of the interaction cavity geometry were retained. The splitter in this second model could be slightly moved prior to the experiments to adjust the symmetry of both sides of the model.

The encapsulated electrodes e_1 and e_2 (named according to Fig. 11), were improvised by cutting a length of 20 mm wide copper foil. Their outer parts, beyond the 38 mm width of the Al_2O_3 barrier plate are seen in Figs. 15 and 16 provided with the connectors for applying the electric input signal. The exposed narrow g electrode, a 0.04 mm diameter wolfram wire, is also visible in Figs. 15 and 16. It is seen fixed upstream from the fluidic supply terminal and leading through the supply nozzle and the interaction cavity to a downstream location between the diffusers. It was also provided with connector, used for grounding.

The feasibility tests were not intended to obtain numerical data. The aim was to permit visual inspections of the behaviour. On one hand, the transparent top plate covering the cavities made possible observing the shapes and lengths of the glowing ions trajectories. To evaluate the response of the fluidic side required a detector of the output flow. In this role was used a hot-wire MiniCTA anemometer set as supplied by Dantec, Ltd.. The anemometer probe was 55 P 161, positioned with its tip immediately outside one of the amplifier output exits. The anemometer was not calibrated because its task was merely to indicate on the connected oscilloscope the output signal with timed flow pulse beginnings (the leading edges) and ends (trailing edges). A minor problem was the anemometer cannot discriminate between the positive and negative (suction) flow directions. This somewhat decreased the amplitudes of the oscilloscope traces. Nevertheless the beginnings and ends of the flow pulses were recognisable because the suction velocity was lower.

Despite the limitations of the simple performed tests, the extemporised model made possible obtaining useful information about changes of performance found with varying operational parameters, like the air supply flow rate and frequency of switching the modulating rectangular wavetrain.

3.4 Input signal

The generation of ionic wind was governed by the AC signal applied in an alternating manner to the two encapsulated electrodes. Although working with high signal voltages ΔU is inconvenient, the linear proportionality between the desirably high ionic wind velocity and the voltage eq.(4) indicates that - at least at this stage of not particularly efficient electrode configurations – the high voltage was unavoidable. The voltage used in the experiments with reasonable safety was

$$\Delta U = 5.36 \text{ kV} \qquad (7)$$

These magnitudes in the two control lines were obtained by transformers (one for each electrode pair) which were salvaged from discarded cathode ray tube TV sets (in which they originally served for controlling the movement of the electron beam). The frequency of the control AC signal was f_{AC} = 103.5 kHz.

Because of the dual character of the transducer model, with mutually alternating roles of the active and inactive regimes in its two halves, the AC ionic wind generating input into the transducer consisted actually of two mutually complementary input signal leads, one to each of the encapsulated electrodes. The control over this switching between the electrodes was by a signal generator producing two rectangular wavetrain outputs of adjustable frequency - the same frequency and amplitude in the two inputs. The duty cycle (ratio between pulse duration and the period) was constant 0.5. In other words, the ON pulse fed into the electrode on the inactive side alternated with the simultaneous OFF current pulse on the active side. The bistability offered by the geometry of fluidic cavities was not used – the signal was fed to the electrodes for the while duration of air flow on the active side. This continuous action of the ionic wind (rather than a short switching pulse) was found advisable because of the weak ionic wind which would otherwise had difficulty with overcoming the Coanda effect. The opening of the control nozzle on the active side of the transducer increased the pressure in the recirculation bubble (Fig. 7).

An example of the oscilloscope trace of the control signal led into one half of the transducer is presented in Fig. 18 - with an insert in the bottom part of the picture showing in expanded time scale a detail of the AC component (which was obviously not perfectly symmetric, probably by inheritance of the electric circuit components originally designed for another role.

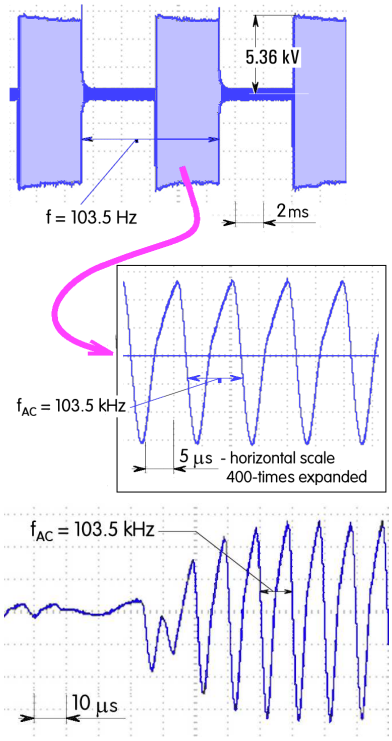

Figure 18: Oscilloscope trace (with expanded detail) of the electric signal used to drive one side of the transducer. This particular trace was recorded at the highest frequency (f = 103.5 Hz) of switching that could be obtained from the available control signal source.

Figure 19: Oscilloscope trace of the electric signal from Fig. 18 with expanded horizontal scale, showing the detail of leading edge of the flow-switching pulse.

One of the most important performance criterion of the transducer model was the clearly defined beginnings and ends of the generated output flow pulses. The next Fig. 19 shows in an expanded time scale the part of the oscilloscope trace at the leading edge of the electric input pulse. The situation at the leading edge is somewhat and in Fig. 19 the real beginning of the pulse may be somewhat uncertain - nevertheless this is the consequence of the very large time scale expansion. The very well defined ON conditions were actually attained already after ~ 30 μs, which is a negligible part of even the shortest pulses.

4. Experiments with second model

4.1. Improvements

The properties of the first model were not investigated in detail since it was expected that the full potential of this type of E/F transducers will be found in the planned second, advanced model. In the meantime, rather positive experience with the first model became accumulated and this has led to adopting into the second model many more aspects – including the geometry of the interaction cavity, Fig. 17, and also the complete Al_2O_3 barrier plate — than was originally envisaged.

It has to be taken into account that internal geometry of fluidic valves has a very large number of variable parameters, mutually related by non-linear dependences – a number so large that geometry optimisations in fluidics are still rather impractical. Developments are currently still done as small shape changes that experience has found successful, cf. e.g. [23]. After all, the geometry presented in Fig. 17 was inherited from a long line of only slightly changed earlier fluidic amplifiers discussed, e.g., in [21], [22], [23] — all stemming from the early ancestor presented in [24]. Since the experience with the fluidic properties of the preliminary model was quite good, the key central part of the interaction cavity was retained.

Of the changes that were made is immediately apparent in the photographs of the new second model in Figs. 20 and 21. It is the elimination of diffusers. Because of the use of velocity sensing anemometer as the detector for evaluation of performance, the pressure increase at the price of decreasing velocity in a diffuser was contra-productive. The other visible change in the second model is separation of the splitter from the rest of the main plate. This makes the splitter position adjustable so as to obtain symmetry of properties of both sides of the device. The symmetry was previously not satisfactory because of the manufacturing tolerances of the external laser cutting supplier.

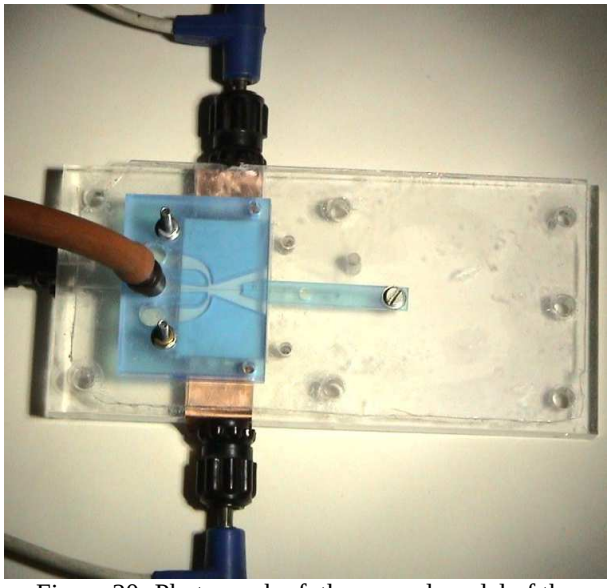

Figure 20: Photograph of the second model of the transducer used in the experiments. Note the splitter held by the single screw so that it could be nudged for adjustment of symmetric behaviour.

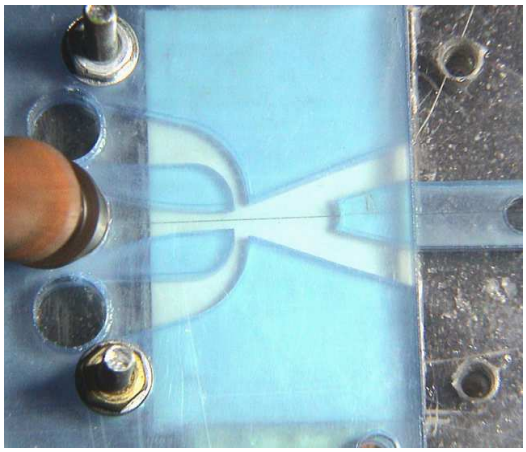

Figure 21: Detail photograph of the interaction cavity in the second transducer model. Clearly recognisable is here the thin wolfram wire electrode passing through the whole length of the interaction cavity.

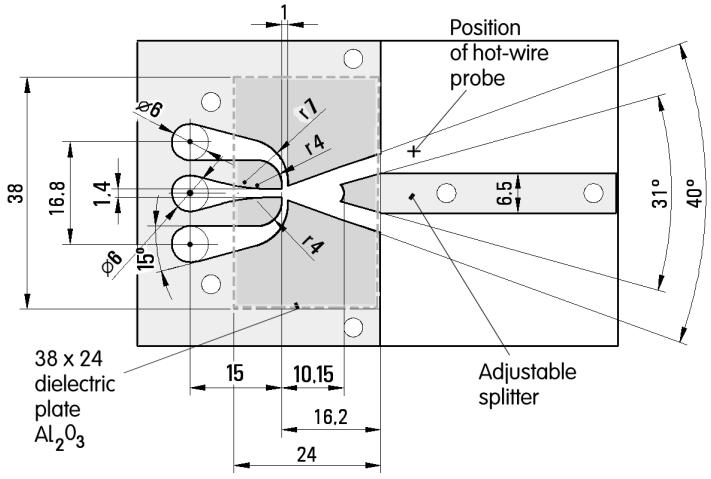

Figure 22: Geometry of the second, improved laboratory model. Because of favourable previous experience with the extemporised first model, key parts of the interaction cavity geometry (Fig. 17) were inherited. The splitter could be slightly moved prior to the experiments to obtain symmetric behaviour of both sides of the model

Particularly satisfactory with the feasibility tests of the first model was the Al_2O_3 barrier plate. The new version was initially designed not only to use the same plate but also to increase sensitivity of the E/F signal conversion by placing on top of the main plate – the one with the laser-cut cavities - another, second barrier plate with the same set of electrodes. This would double the intensity of the generated ionic wind, acting in the upper half of the interaction cavity space not influenced by the bottom plate. As is apparent in Figs. 20 and 21, the placement of this plate would cover the control nozzles, which were found necessary for proper transducer operation. To make the placement possible (drilling holes in the barrier would be difficult - and undesirable, since it would disrupt the barrier effect) the control nozzles in the new geometry, presented in Fig. 22, were made longer and bent so that their inlet holes were away from the area covered by the barrier plate. The atmospheric inlet holes were then side by side with the supply terminal.

In the end, circumstances prevented the use of the second barrier plate – mainly because of its lack of transparency. Observation of the plasma was useful for adjusting the transducer. The configuration of the electrodes was thus also left the same as before.

4.2 Results

Targets aimed at in the experimental investigations with the improved second model were as follows:

(a) Reasonable response to the electric input in the form of more or less rectangular-shaped fluid flow output pulses.
(b) Operation at input pulses frequency $f > 100$ Hz
(c) Capability of operating also at low Reynolds number values, $Re < 1000$ (for use of scaled-down devices in microfluidics)
(d) Small required supply pressure levels, $\Delta P < 100$ Pa

Attainment of these goals was evaluated by inspection of the oscilloscope trace of the output signal of an non-calibrated hot-wire anemometer. The approximate position of the anemometer probe is indicate in Fig. 22. Calibration – and conversion of the anemometer electric output signal into velocity values — were unnecessary since the purpose of the anemometer was just to detect the beginnings and ends of the flow pulses. The criterion of success was regularity of the pulses and no missing pulse. Because of the inability of hot-wire measurement to detect the sign (negative or positive flow), the pictures of the flow pulses – as they are shown, e.g., in Fig. 23 – are somewhat misleading – the "zero flow" between the individual pulses is actually the response to non-zero suction flow on the inactive side. In other words, the actual heights of the pulses are higher than is suggested by the impressions from the oscilloscope traces presented in Fig. 23. More important fact about the pulse heights is the comparison in Fig. 23 between the pulse repetition frequency $f = 79.6$ Hz (above) and $f = 103.5$ Hz (below). Circumstances did not allow testing the model at frequencies higher than these. Nevertheless, since there is no recognisable difference in the higher and the 1.35-times higher frequency lower trace, it is evident that the transducer model would be able to operate equally well even at repetition frequencies substantially higher.

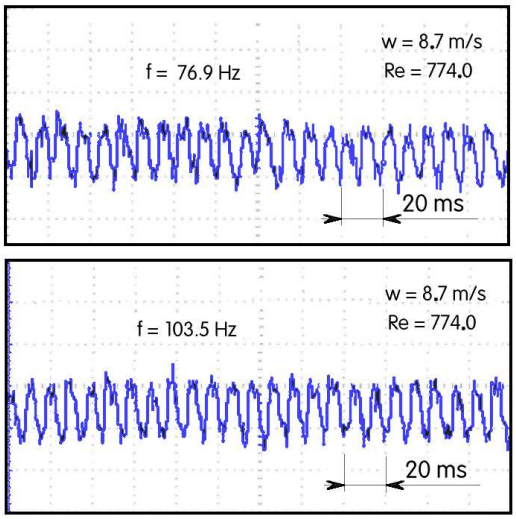

Figure 23: Proof of attaining the planned goals: two examples of generated flow pulses in the output terminals. Sensor used was a non-calibrated hot-wire anemometer. The velocity w is the bulk value computed (neglecting the existence of boundary layers) for the conditions inside the exit from the supply nozzle

Experience gained in the experimentation shows that the key factor for success is proper choice of the combination of the driving voltage, eq. (7), and the supply flow rate, which was 0.029 g/s in the experiments of Fig. 23 (alternatively, the second parameter to be matched may be the bulk velocity w in the supply nozzle exit). The combination of values mentioned above was found to be optimal by cut-and-try approach. If the supply flow rate were higher than this optimum, the ionic wind did not suffice for switching the air jet into the other output terminal. If the mass flow rate was lower, the decreased Reynolds number has led to irregularities in the generated pulses, indicating the loss of the Coanda effect attachment – after all, in investigation of very similar model of bistable diverter discussed in [20] it was concluded that the attachment necessitated Reynolds number above $Re \sim 800$.

5. Conclusions

Direct action of an electric input signal on an air flow in a fluidic element – i.e. without any action of mechanical moving components - has been a dream of a whole generation of fluidic device designers. Current successful employment of fluidic devices is a number of useful application made the conversion task of increasing urgency. This paper presents a solution based on generation of non-temperature plasmonic wind between electrodes – one wide planar and the other very narrow wire (strip). The starting point of the design was standard fluidic bistable diverter amplifier. The main factor in the device design was simplicity and the electrode configuration did not promise particular efficiency. Nevertheless, the demonstrated signal converting performance was found quite good, with fair perspective of use in applications.

Acknowledgments

Authors' research was supported by grant 13-2304S obtained from GAČR. They were also recipients of institutional support RVO: 61388998.

References

[1] "*Microfluidic systems for combinatorial chemistry*", in Encyclopedia of Microfluidics and Nanofluidics, Dongqing Li (Ed.), Springer-Verlag, Berlin, New York, Heidelberg 2008

[2] Chapter #5 in: Tesař V.: "*Pressure-Driven Microfluidics* ", Artech House Publishers, Norwood, MA 02062 USA, 2007

[3] Tesař V.: " *Způsob a zařízení k ovládání průtoku tekutiny*" (Ways and means for controlling fluid flow – in Czech), Czechoslovak Patent 141005, filed Nov. 1970

[4] Tesař V.: „*The Guided Jet Principle*", Fluidics Quarterly, Vol. 3, p. 77, 1971

[5] Gregory J.W., Gnanamanickam E.P., Sullivan J.P., Raghu, S, "*Variable-frequency fluidic oscillator driven by piezoelectric devices*", Proc. of 43rd AIAA Aerospace Sciences Meeting, Reno, NV., 2005

[6] Tesař V.: "*Převodník proudového typu pro převod elektrického signálu na signál fluidický*" (Jet-type transducer for converting an electric signal to a fluidic one – in Czech), Czechoslovak Patent 148724, filed June 1972

[7] Tesař V.: *"Control of flow separation by temperature gradient"*, Proc. of Euromech Colloquium 377 Stability and Control of Shear Flows with Strong Temperature or Density Gradients, Praha, May 20-22, 1998

[8] Turck J.: „*Procédé et dispositif pour influencer l'ecoulement dun fluide le long d'une surface, par exemple une surface alaire*" (Ways and means for influencing a fluid flow along a surface, for example a sirface of a wing – in French), French Patent 1031925, filed Jan 1951

[9] Bahnson A.H.: "*Appareil pour produire une poussée lorsqu'on applique une tension électrique à ses électrodes*" (An apparatus for generating a pressure by applying a voltage on electrodes – in Frech) , French Patent 1266476, filed May 1959

[10] Hill G.A.: „*Ioinized boundary layer fluid pumping system*", US Patent 3,095,163, filed 1963

[11] Roth J.R.: "*Method and apparatus for covering bodies with a uniform flow discharge plasma and application thereof*", US Patent 5,669,583, 1997

[12] Roth J.R.: "*Industrial Plasma Engineering: Vol. 2: Applications to Nonthermal Plasma Processing*", Institute of Physics Publishing Ltd., London 2001

[13] Roth J. R., Sherman D. M., Wilkinson S. P. „*Boundary layer flow control with a one atmosphere uniform glow discharge surface plasma*", AIAA Meeting (Reno, USA) paper #98-0328 : 1998

[14] Wang J.-J., Choi K.-S., Feng L.-H., Jukes T. N., Whalley R.D.: "Recent developments in DBD plasma flow control", Progress in Aerospace Sciences, Vol. 62, p. 52, 2013

[15] Moreau E.: "*Airflow control by non-thermal plasma actuators*", Journal of Physics D: Applied Physics Vol. 40, p. 605, 2007

[16] Gregory J., Ruotolo J.C., Byerley A. R., McLaughlin T.E.: "*Switching behavior of a plasma-fluidic actuator*", Proc. of 45th AIAA Aerospace Sciences Meeting & Exhibit (AIAA 2007-0785), Reno, NV., USA 2007

[17] Tesař V., Šonský J.: "*Způsob a zařízení k rozvádění tekutiny v závislosti na elektrickém řídicím signálu*" (Ways and means of distributing a fluid in dependence upon an electric control signal – in Czech), Czech Patent Application PV 2013, Dec. 2013

[18] Tesař V.: "*Skin friction sensor suitable for extreme conditions"*, Flow Measurement and Instrumentation, Vol. 33, pp. 228-238, 2013

[19] Tesař V., Zhong S., Fayaz R.: „*New fluidic oscillator concept for flow separation control*", AIAA Journal, Vol. 51, p. 397, 2013

[20] Tesař V., Bandalusena H.: „*Bistable diverter valve in microfluidics*", Experiments in Fluids, Vol. 50, p. 1225, 2011

[21] Tesař V., Hung C.-H., Zimmerman W. „*No-moving-part hybrid-synthetic jet actuator*". Sensors and Actuators A: Physical, Vol. 125, p. 159, 2006

[22] Tesař V. et al.: "*Experimental investigation of a fluidic actuator generating hybrid-synthetic jets*", Sensors and Actuators A: Physical, Vol. 138, p. 213, 2007

[23] Tesař V.: "*Fluidic control of reactor flow – Pressure drop matching*", Chemical Engineering Research and Design, Vol. 87, p. 817, 2009

[24] Tesař V.: "*A mosaic of experiences and results from development of high-performance bistable flow-control elements*", in: Proceedings of the Conference on Process Control by Power Fluidics, Sheffield,UK, 1975

[25] Rickard M., Dunn-Rankin D., Weinberg F., Carleton F.: „*Characterisation of ionic wind velocity*", Journal of Electrostatics, Vol. 63, p. 711, 2005

[26] Chattock A.: „*On the velocity and mass of ions in the electric wind in air*", Philosophical Magazine, Vol. 48, p. 401, 1899

[27] Tesař V., Tippetts J.R., Allen R.W.K., Low Y.Y.: "*Subdynamic asymptotic nehaviour of microfluidic valves*", Journal of MEMS, Vol. 14, p. 335, 2005

[28] Hardy P., et al.: „*Plasma synthetic jet for flow control*", AIAA paper 2010-5103

[29] Grossman K. R., , et al.: „*Characterization of SparkJet actuators for flow control*". AIAA paper 2004-89

[30] Belinger A., et al.: „*Plasma synthetic jet actuator: electrical and optical analysis of the discharge*", Journal of Physics D: Applied Physics, Vol.47, 245202, 2014.